Chemical Engineering Journal 142 (2008) 337–343

Contents lists available at ScienceDirect

Chemical Engineering Journal

journal homepage: www.elsevier.com/locate/cej

# Synthesis of two-dimensional ZnO nanopellets by pyrolysis of zinc oleate

W.S. Chiu [a], P.S. Khiew [a,*], D. Isa [a], M. Cloke [a], S. Radiman [b], R. Abd-Shukor [b], M.H. Abdullah [b], N.M. Huang [b]

[a] Faculty of Engineering, University of Nottingham Malaysia Campus, Jln Broga 43500, Semenyih, Selangor Darul Ehsan, Malaysia
[b] School of Applied Physics, Faculty of Science & Technology (UKM), Universiti Kebangsaan Malaysia, 43600 Bangi, Selangor Darul Ehsan, Malaysia

ARTICLE INFO

*Article history:*
Received 17 March 2008
Received in revised form 23 April 2008
Accepted 25 April 2008

*Keywords:*
Characterization
Crystal morphology
Growth from solution
Zinc oxide
Semiconducting II–VI materials

ABSTRACT

We report the non-hydrolytic solution phase synthesis of two-dimensional zinc oxide (ZnO) nanopellets by using self-made organometallic compound (zinc (II) oleate, $Zn(C_{18}H_{33}O_2)_2$) as single precursor. $Zn(C_{18}H_{33}O_2)_2$ is prepared by ion exchange reaction between non-toxic fatty acid (palm oil extract) and ion $Zn^{2+}$. The controlling process of thermal pyrolysis of precursor is carried out under inert argon (Ar) atmosphere. This technique is very effective and reproducible in controlling the shape of ZnO semiconductor nanostructures. The as-synthesized ZnO nanocrystals are found in two-dimensionally well-faceted triangular and hexagonal thin pellet structures. Transmission electron micrograph(s) (TEM) show that the morphologies of ZnO nanopellets can be controlled by annealing duration. X-ray powder diffraction patterns reveal that all the peaks of ZnO nanopellets can be well indexed with standard hexagonal phase of ZnO crystal structure.



## 1. Introduction

Nanomaterials have received considerable attention from the scientific and engineering communities due to their novel properties and various techniques have been employed to control their geometrical factors including size and shape. The purposes of these assiduous efforts are to tune and exploit various anomalous shapes dependent properties of nanomaterials. For instances, Wang et al. have observed unusual polarization anisotropy properties of indium phosphide (InP) nanowires synthesized by laser-assisted catalytic growth and these nanowires have subsequently been utilized in fabrication of polarization-sensitive nanoscale photodetectors [1]. In addition, Zhong et al. have prepared high quality single crystal p-type gallium nitride (GaN) semiconductor nanowires by chemical vapor deposition (CVD) and technically applied it as nanoscale UV–blue LEDs [2]. Further to this, Hahm et al. have also reported p-type silicon nanowires that have been grown by CVD and they chemically incorporated these materials in ultra-sensitive electrical detection of DNA [3].

Nowadays, the innovative application of nanomaterials in the design of electronic devices is massively dependent on the congruent electronic properties of the selected nanomaterials. However, the electronic property is highly influenced by the structural dimension of the nanomaterials. Regarding to the structural dimension of nanomaterials, for 1D semiconductor nanostructures, the quasi-continuous density of states exhibits singularities near the band edges followed by exponentially decay while that of 2D semiconductor nanostructures is partially discrete [4,5]. Substantial variation in electrical and optical properties in accordance to the dimensional changes can be observed when the particular electronic energy gap exceeds the thermal energy. Some examples of remarkable 2D quantizes effects are integer and fractional quantum hall effects [6–9]. Therefore, a routine method in preparing 2D semiconductor nanostructures should be developed to unravel the shape-guiding effects.

Generally, there are two renowned synthetic approaches used in preparing desirable semiconductor nanostructures of the nanomaterials for the application purposes. One synthetic approach is gas-phase synthesis while another is solution-phase synthesis. For most of 1D nanowires which prepared by gas-phase synthesis, the major limitation subjected to this synthetic approach is low yield and consuming large amount of thermal energy. Thus, it becomes an obstacle for large-scale production. In contrast to this gas-phase synthesis, the problem mentioned above can be solved in solution-phase synthesis. Additionally, solution-phase synthesis offers a more economical route, high throughput and large-scale production of high quality nanostructures that are monodisperse in shape and size [10–12]. For example, by scrupulously controlling the chemical reaction in solution-phase synthesis, Law et al. have successfully boosted the aspect ratio of ZnO nanowires above 125 and tremendously increased the yield. Furthermore, this topology is found to improve the quantum efficiency of dye-sensitized solar cells (DSCs) in the red region of the spectrum in order to attain the full sun efficiency up to 1.5% [13]. Thus, solution-phase syn-

* Corresponding author. Tel.: +60 3 89248179; fax: +60 3 89248017.
*E-mail address:* PoiSim.Khiew@nottingham.edu.my (P.S. Khiew).

1385-8947/$ – see front matter © 2008 Elsevier B.V. All rights reserved.
doi:10.1016/j.cej.2008.04.034

thesis provides a facile and controllable route in synthesis of novel nanomaterials.

Recently, oxide-based semiconductor nanomaterials also become subject of study due to their thermal- and photo-stability [14]. Among these nanomaterials, ZnO is the well-known candidate due to its relatively wide band gap energy (3.37 eV). This property enables the ultraviolet lasing effects to be observed at room temperature [15–17]. In addition, the exciton binding energy of ZnO (60 meV) is much larger than thermal energy at room temperature (26 meV) if compared to that of the other semiconductor materials such as ZnSe (22 meV) [18] or GaN (25 meV) [19]. The latest study found by Garcia et al. indicates that ZnO nanocrystals also exhibit interesting ferromagnetic-like behavior at room temperature even though in the absence of dopants. The anomalous magnetic property is attributed to the binding effects of capping ligands that greatly alter the electronic structures of ZnO [20]. Moreover, various research groups have successfully exploited the novel semiconductivity properties of ZnO for advance technological applications. For examples, Huang et al. firstly reported blue nanolaser under optical excitation at wavelength of 385 nm by using ZnO nanowires as natural cavities even though it is at room temperature [21]. Recently, Wang et al. have created an interesting direct-current nanogenerator, which is using ZnO nanowires arrays and driven by an ultrasonic wave, has shown useful application of ZnO nanostructures. The vibration resulted from the interaction of nanowires and ultrasonic waves, causes piezoelectric semiconducting coupling process to occur and converts mechanical energy of nanowires to electrical energy [22].

Most of the novel and well-defined ZnO nanostructures are in 1D [14,23–25]. As a consequence, the intensive studies on 1D nanostructures have caused the development of 2D ZnO nanostructures to lag behind. At the same time, there are limited reports on the synthesis of 2D ZnO nanostructures by solution phase, as well as the utilization of 2D nanostructures for nanodevices designs. Currently, most of the studies on 2D ZnO semiconductors have been done on nanostructures, which usually form at interfaces, are hardly prepared by using sophisticated instrument such as molecular beam epitaxy (MBE).

In fact, although there has been a great deal of recent works on ZnO semiconductors, the researches are still considerably lagging behind the state of the art of chalcogenide-based semiconductor nanostructures. This phenomenon could be attributed to the poor synthesis method and less suitably applicable capping ligands (only used in solution-phase synthesis) for high temperature synthesis process while this high temperature synthesis process (in gas-phase synthesis) is favored for oxidation reaction to occur. On the other hand, the apparatus setup of such high temperature reactor for gas-phase synthesis of ZnO nanostructures is very complex. Meanwhile in solution-phase synthesis of ZnO nanostructures, the unsuitable surfactant template like microemulsion or lamellar structures tends to rupture at such high temperature [26–34]. Consequently, all the obstacles mentioned above in both gas- and solution-phase syntheses have limited the studies of 2D ZnO nanostructures.

In this paper, we report the shape control solution-phase synthesis of 2D ZnO nanopellets using thermal sustainable organic compound (oleic acid) as capping ligands. We have found that oleic acid is an effective capping ligand in preparing 2D ZnO semiconductor and no agglomerations are found even though the temperature of the system is heated to 317 °C. The precursor (zinc (II) oleate, $Zn(C_{18}H_{33}O_2)_2$) and capping ligands are fatty acid compound, which are respectively originated from natural palm oil with lower toxicity. Besides that, the as-synthesized 2D nanopellets have well-defined shape either in triangular or hexagonal pellet with average edge length of 30–150 nm. In comparison with other synthetic approaches in producing 2D ZnO nanopellets [35,36], current synthetic approach offers an effective route to produce 2D nanopellets which are smaller and well-defined shapes. The edge lengths and thickness are less than 100 and 10 nm, respectively. The nanopellets are well-separated with each other without stacking effect as reported by Yoshida et al. [37]. Furthermore, the as-synthesized nanopellets are stable in terms of chemically and physically if compared to previous report [38] even though undergoes several drying and dispersing process repeatedly. In addition, the current synthetic approach offers an inexpensive, safe and facile synthesis route to produce ZnO nanopellets with high yield if compare to gas-phase synthesis such as MBE [39].

## 2. Experimental details

### 2.1. Synthesis of zinc (II) oleate ($Zn(C_{18}H_{33}O_2)_2$) precursor

The zinc (II) oleate precursor was prepared by ion exchange reaction between Zn (II) chloride hexahydrate ($ZnCl_2{\cdot}6H_2O$) and potassium oleate ($C_{18}H_{33}KO_2$). Schematic flow chart for the ($Zn(C_{18}H_{33}O_2)_2$) precursor preparation is depicted in Fig. 1. All the chemicals were used without further purification. Firstly, 0.05 mol $ZnCl_2{\cdot}6H_2O$ (Fluka, 99%) and 0.1 mol $C_{18}H_{33}KO_2$ (Fluka, 99%) were mixed with solvent consisted of 100 ml ethanol ($C_2H_5OH$, 99.5%), 175 ml *n*-hexane (Mallinckrodt, 100%) and 75 ml ultrapure deionized water (resistivity = 18.2 MΩ, Deionizer Purelab Prima Elga). The mixture was loaded into a two-neck flask to which was equipped with condenser and thermometer before this loaded mixture was refluxed at 80 °C for 2.5 h. Upon heating, the upper organic layer consisting of *n*-hexane turned yellowish and this

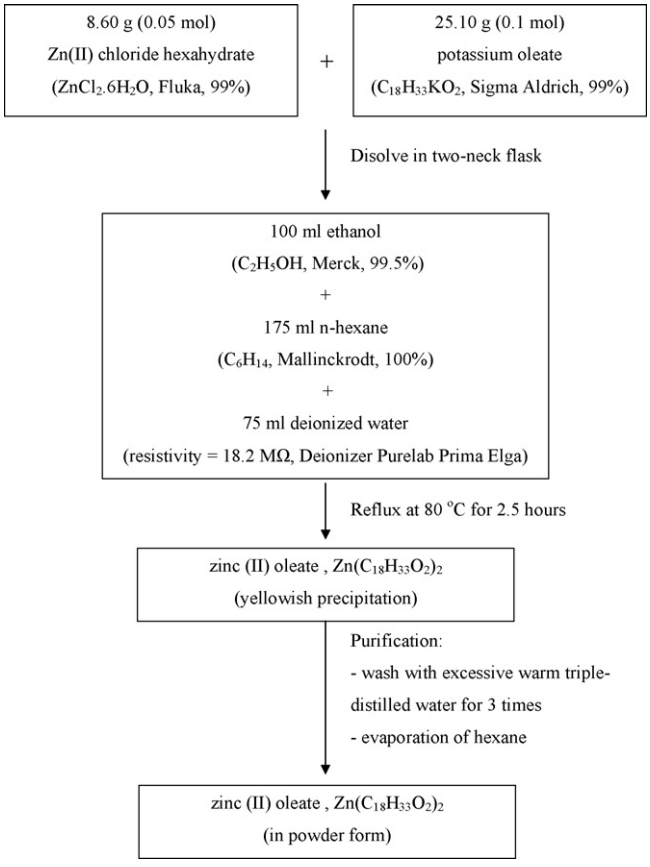


**Fig. 1.** Schematic flow chart for the synthesis of $Zn(C_{18}H_{33}O_2)_2$ precursor.

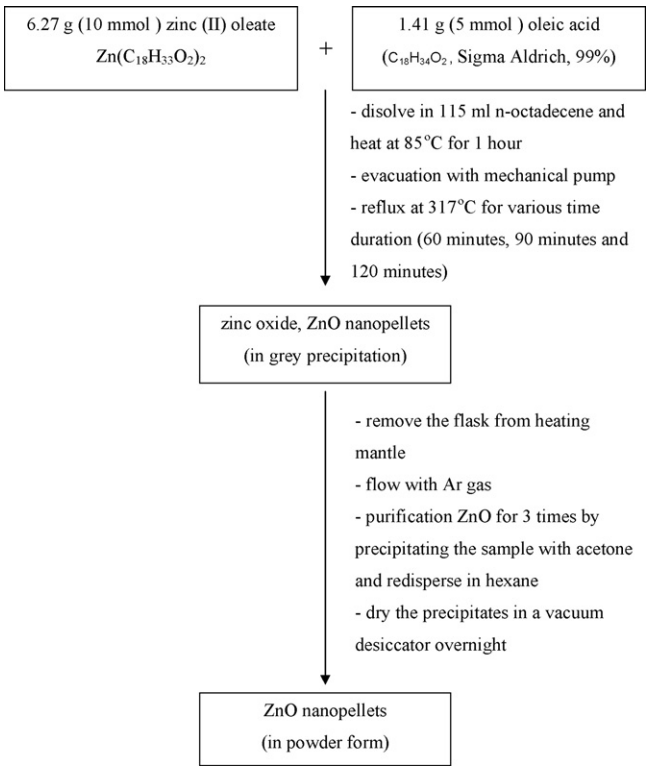


**Fig. 2.** Schematic flow chart for the synthesis of 2D ZnO nanopellets.

was clearly indicating the formation of $Zn(C_{18}H_{33}O_2)_2$. Next, physical separation was done using separation funnel and the $Zn(C_{18}H_{33}O_2)_2$ were repeatedly washed with excess warm triple-distilled water to remove the unreacted metal salts. After washing process, hexane was evaporated off with a rotavapor, resulting in organometallic compound of $Zn(C_{18}H_{33}O_2)_2$ in the powder form.

### 2.2. Synthesis of 2D ZnO nanopellets

Schematic flow chart for the synthesis of 2D ZnO nanopellets is shown in Fig. 2. The reaction was carried out in a 250 ml four-neck flask equipped with a condenser in an inert Ar atmosphere. The heating mantle equipped with magnetic stirrer was used to provide local hot spot to the wall of the reactor under vigorous stirring. The apparatus setup for the synthesis of ZnO nanopellets is shown in Fig. 3. In a typical synthesis, 10 mmol $Zn(C_{18}H_{33}O_2)_2$ and 5 mmol oleic acid ($C_{18}H_{34}O_2$, Sigma–Aldrich, 99%) were dissolved in 115 ml *n*-octadecene after being continuously heated at 85 °C for 1 h. Afterwards, evacuation was done repeatedly with mechanical pump to eliminate the oxygen and residual water. Then, the temperature of the mixture was ramped to 317 °C with a constant heating rate and refluxed for various time duration (60, 90 and 120 min). The presence of grey precipitation indicates the formation of ZnO nanopellets.

The refluxing processes for samples heated with 60, 90 and 120 min were terminated by removing the flask from the heating mantle and the mixture was cooled by continuous flow of Ar gas until room temperature. The grey precipitates were obtained by adding excess amount of non-solvent (acetone) and typical non-polar solvent (hexane) was added to redisperse the precipitates. The processes of precipitating and dispersing were repeated for three times to remove the impurities. Finally, the precipitates were dried in a vacuum desiccator overnight.

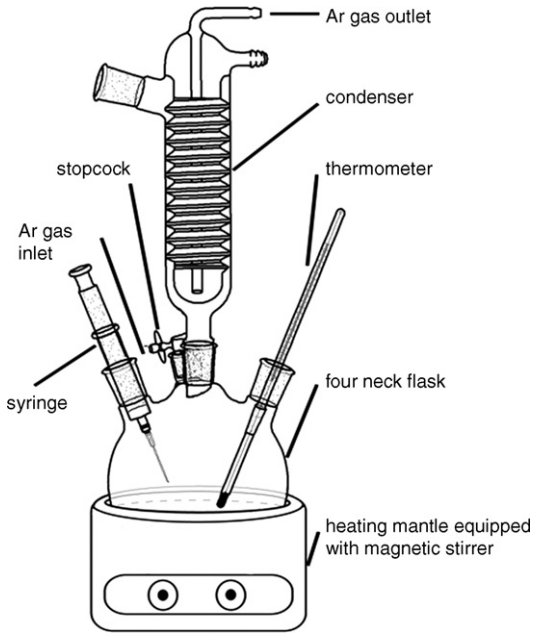


**Fig. 3.** Apparatus setup for the synthesis of ZnO nanopellets.

The morphology of 2D ZnO nanopellets was characterized by transmission electron microscope (TEM) (Philips CM12 with operation voltage 100 kV) while X-ray diffraction (XRD) was used to identify the crystal structures by using Bruker AXS-D8 Advance Diffractometer (scanning rate 0.01°/s, Cu Kα radiation and wavelength, $\lambda = 0.154$ nm). The element analysis was performed by energy dispersion X-ray analysis (EDXA) by using Leo 1450 VPSEM instrument operated with acceleration voltage 15 keV.

## 3. Results and discussion

Fig. 4 shows the TEM micrograph of ZnO crystals annealed at 317 °C for 60 min. The average edge length is between 30 and 120 nm. Typically, the crystals exist in 2D pellets with irregular shapes. The surfaces of the nanopellets are rough and stacked with many primary grains, which could be attributed to incomplete atomic diffusion. The densities of small primary grains for some of the nanopellets are high along their edges if compared to that of their center as can be seen in TEM micrograph (Fig. 4). Subse-

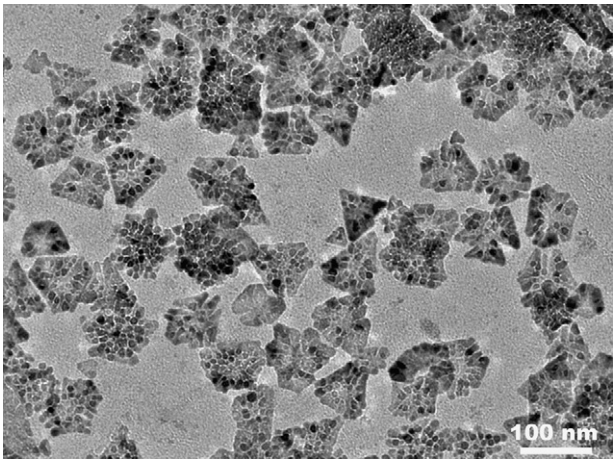


**Fig. 4.** TEM micrograph (magnification 35,000×) of ZnO nanopellets annealed at 317 °C for 60 min.

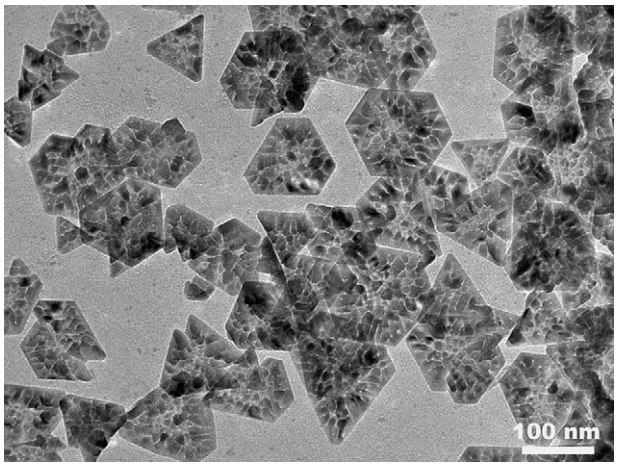


**Fig. 5.** TEM micrograph (magnification 35,000×) of ZnO nanopellets annealed at 317 °C for 90 min.

quently, the transmission of electron beam is greatly hampered due to the absorption of the electrons by the sample especially at the edge of the nanopellets. The contrast of the micrograph implies the ununiformity of the sample with a wedge at the center of the nanopellets.

In comparison with other similar studies which have adopted solution-phase synthetic approach, Yoshida et al. reported the formation of 2D ZnO nanopellets with the assistance of water-soluble tetrasulfonated metallophthalocyanines (TSPsMs where M = $Zn^{2+}$, $Al^{3+}$, $Si^{4+}$) as capping ligands [37]. However, the use of TSPsMs only can produce ZnO nanopellets with thickness around 1 μm. This could be attributed to the "bridging effect" of TSPsMs that allows the further growth of new ZnO disk planes on it and this "bridging effect" subsequently causes the stacking disks structure to be observed. Different from the capping ligands (TSPsMs) mentioned, the as-synthesized ZnO nanopellets in this article by using oleic acid as capping ligands manage to tune the nanopellets with thickness less than or equals to 10 nm which is much thinner. Besides the difference mentioned above, the growth of the primary nuclei along *c*-axis is inhibited due to the adsorption of oleic acid to the corresponding surface of the growing crystal, where no "bridging effect" has been observed as oleic acid provides greater stearic hindrances to inhibit the deposition of new plane on the initial disk plane.

According to the recent literature reports, oleic acid that functions as coordinating agent can selectively bind on the specific crystal face(s) to regulate the growth and the orientation of the particular crystal face(s) kinetically [40–43]. Detailed studies by Wang et al. reveal that ZnO are highly polarized materials with chemically active $Zn^{2+}$ terminated ZnO (0 0 0 1) polar surface while the $O^{2-}$ terminated (0 0 0 $\bar{1}$) polar surface is inert [44]. Therefore, control ramp of the temperature in our sample caused $Zn(C_{18}H_{33}O_2)_2$ to decompose and the constituent cation ($Zn^{2+}$) deposited on the ZnO nuclei, while the negative charge alkyl chain ($(C_{18}H_{33}O_2)^-$) was found strongly bound on the highly polarized $Zn^{2+}$ surface. As a result, further crystal growths occurred via continuous deposition of constituent element $Zn^{2+}$ along *a*-axis and *b*-axis rather than *c*-axis, this clearly explains the primary ZnO crystals exist in 2D thin pellet form with higher grain density along the edge of the crystal rather than that of the center (Fig. 4).

With increasing duration of annealing to 90 min, the nanopellets exist in more well-defined shapes with flat edges (Fig. 5). This sample has shown "shape distribution" with the presence of both triangular and hexagonal nanopellets. The average edge length of this sample (90 min) is more than that of the sample being annealed for 60 min. The edge length of this sample falls within the range of 40–125 nm. The densities of the primary grains on the edges of the nanopellets become lower and this could be attributed to the complete atomic diffusion process.

During the refluxing process, the tendency in minimizing the overall surface energy had caused the atomic diffusion, which subsequently decreased the surface area of the primary grains [45–47]. The primary grains along the edges of the individual crystal were highly unstable due to the low atomic packing density. The morphologies obtained from the 90 min sample were believed to provide higher energy areas that promoted grain boundary formation. After the sample exposed to a finite cumulative period of annealing for 90 min, the thermal energy absorbed had sufficiently triggered the surface atomic migration, followed by reorganization of the atom into the correct positions where the crystal lattices were formed. Subsequent thermal annealing caused the coalescence of small grains to form rather than big grains. These bigger grains were separated by the grain boundaries on the surface of the nanopellets as the result of thermally activated mass transport process. With prolonged annealing, the coalescence among the grain boundaries had caused the emergence of the strong texturing surface. The sintering effect of the grains can also be observed from Fig. 6(a), which has shown rather smooth surfaces along the grain boundaries where the energy was reduced. This phenomenon is well-correlated with molecular dynamics simulations reported by Zhu et al. [48].

In order to investigate the effects of annealing duration on the shape of nanopellets, we have performed high magnification of TEM to observe the surface morphology on the selected ZnO nanopellets that were annealed for various times (Fig. 6). According to Fig. 6(a), the ZnO nanopellets are triangle in shapes with flat equilateral edge. The truncated edge is also observed along each corner of the triangular nanopellet (highlighted in Fig. 6(a)). Fig. 6(b) has shown one of the "diamond shape" nanopellets with improved truncated edges. These improved truncated edges are to minimize the surface energy of the particular crystal due to the reason that the sharpening corner is highly unstable and requiring large amount of energy to retain its form [49]. On the other hand, these truncated edges are believed to greatly and beneficially affect the absorption and scattering of light, which subsequently offer a new route for 2D ZnO nanostructures in optimizing the plasmon resonance for molecular detection as well as spectroscopy [50].

In the basis of the TEM image statistics, not much substantial difference on the average edge length of ZnO nanopellets has been observed between the samples annealed for 90 and 120 min. The major morphological difference between these two samples is how critical the wedging formed at the center of nanopellets, while the one becomes more critical will eventually lead to the formation of a hole at the center (Fig. 6(c and d)) as a result by the continuous etching reaction of oleic acid on the bare (0 0 0 $\bar{1}$) surface. At the same time, Leng et al. and Samia et al. also observed the etching reaction caused by oleic acid during the preparation of Ni nanosheets and Co nanocrystals respectively [51,52]. We believe by scrupulously controlling the reaction environment, the so-called new family of ZnO nanoring [53] that were prepared by gas-phase synthesis previously can also be prepared by solution-phase synthesis.

Fig. 7 shows the XRD pattern of ZnO annealed for 60 and 90 min. All the peaks can be indexed to that of the standard ZnO with hexagonal wurtzite crystal structures (with space group *P63mc*) [54]. Besides, no diffraction peaks from other impurities have been observed. This implies that all the $Zn(C_{18}H_{33}O_2)_2$ are fully decomposed into ZnO. Both samples shown in Fig. 7 merely consist of wurtzite crystal structures without any presence of zinc blende structures. This is because wurzite structure configuration has the

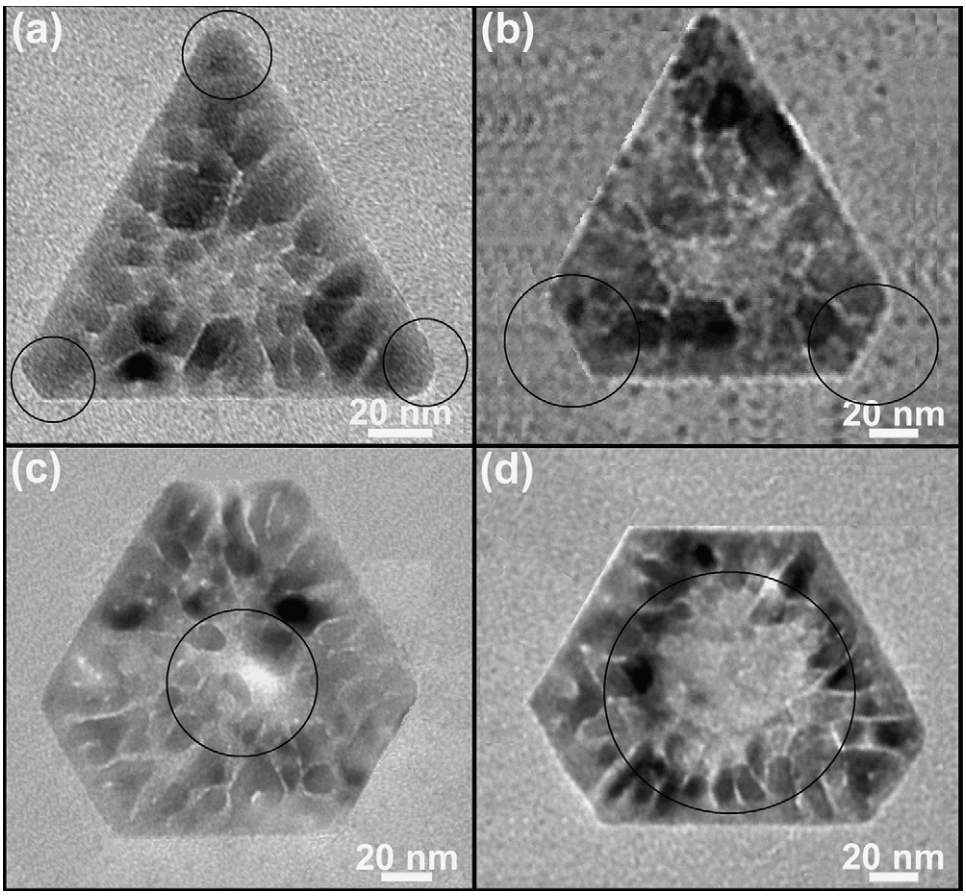


**Fig. 6.** Shape evolution of 2D ZnO nanopellets annealed for 90 min (a and b) and 120 min (c and d). (a) The highlighted circles indicate the truncated edges for a triangle nanopellet. (b) Diamond shape nanopellet with two truncated edges. (c and d) show the formation of a hole at the center of hexagonal nanopellets to form "ring structure" due to the etching effects of oleic acid.

Madelung constant 0.2%, which is larger than that of zinc blende. Thus, the strong ionic compound likes ZnO favors for wurzite structures unless high pressure is applied [55–57].

By choosing the most dominant peak ($hkl$ plane = 1 0 1), we have performed the d-spacing calculations to determine the purities of the samples. The d-spacing based on Bragg's equation ($d_{101} = n\lambda/2\sin\theta$) for our samples annealed with 60 and 90 min is 2.49 and 2.47 Å, respectively. These values are comparable with that of the standard sample (2.48 Å) calculated from standard equation of hexagonal phase ZnO crystal structure ($d_{101} = a/\sqrt{(4/3)(h^2+hk+k^2)+l^2(a^2/c^2)}$) [58]. With increasing annealing duration from 60 to 90 min, the reflective intensities from all the peaks are increased due to the improvement of the atomic ordering. This is attributed to the thermal energy activation that triggered the internal atomic diffusion to the correct position, which also assisted in developing a well-orientated crystal lattice [59]. These are well correlated with TEM micrograph in Fig. 5 where majority of the nanopellets have well-defined shapes with flat edges if compared to sample that was annealed for 60 min (Fig. 4). No phase transitions have been observed, even though after persistent annealing for 120 min was carried out except the increase in the intensity for each peak. In addition, no agglomerations that caused the phase transition were observed from all the samples although the drying and dispersing process were repeated for three times. Explicitly, both of the observations of phase transition above indicate that our nanopellets are more physically and chemically stable if compared to the literature reported [38].

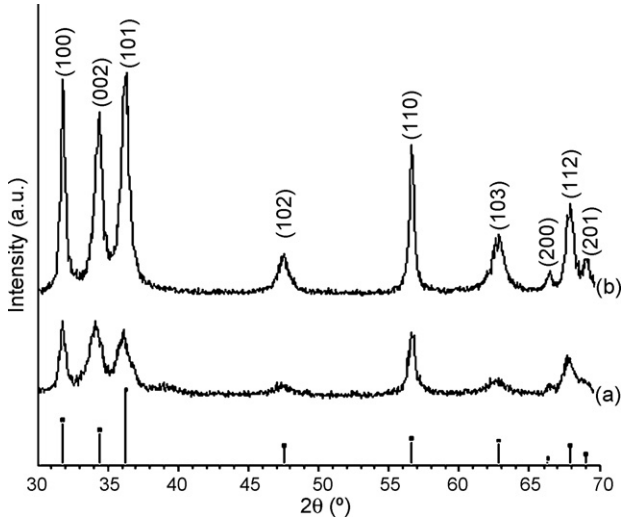


**Fig. 7.** XRD pattern of ZnO nanopellets annealed at (a) 60 min and (b) 90 min ((■) is the standard diffraction pattern).

For sample annealed with 60 min, the relative intensity of the sample does not match with that of the standard sample. In comparison, the sample annealed for 90 min has more well-resolved peaks and the relative intensity of all its peaks matches with the standard diffraction pattern, which indicates the complete growing process. No preferred crystal orientation has been observed to form 1D nanorod as reported [60,61]. The binding effect of oleic acid

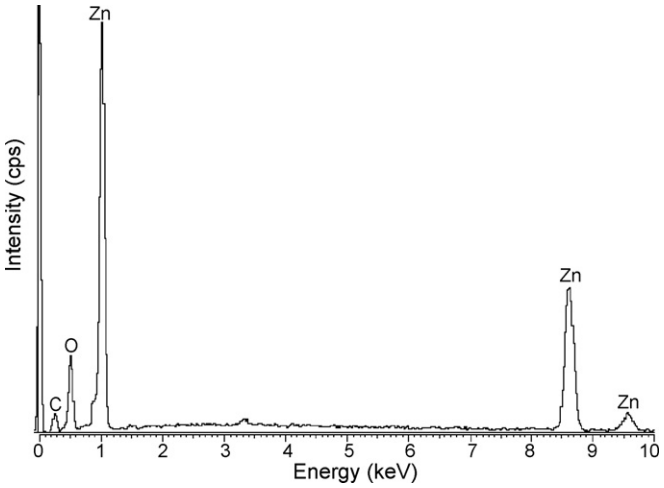


**Fig. 8.** EDXA spetrum of the ZnO nanopellets annealed at 317 °C for 90 min.

on the *c*-axis (0 0 1) is believed to hinder the growth of the crystal orientation and cause the formation of 2D nanopellets, which can be seen in Fig. 4, the primary nuclei exist in 2D pellet form. The initially crystalline phase of the nuclei at the nucleating stage will direct the shapes of the crystals due to its characteristic unit cell structure. Additionally, binding effects of the oleic acid on the primary nuclei have lowered the surface energy of *c*-axis. This causes the realignment of the atoms which constitute the unit cell. As a consequence, the overall surface energy promotes the anisotropy growth of the crystal along *a*- and *b*-axis instead of *c*-axis in order to adapt to its new environment and nanopellets are formed [62].

Fig. 8 shows the elemental analysis for ZnO nanopellets annealed for 90 min. The EDXA spectrum reveals that the samples only consist of Zn, O and C. No other impurities have been detected except for the C molecules which were originated from the residual surfactant molecules on the surface of the ZnO nanopellets. The spectrum shown in Fig. 8 is well-complemented with the XRD measurement as it clearly shows that most of $Zn(C_{18}H_{33}O_2)_2$ constituents have been completely removed from the sample. The average atomic ratio of Zn:O, as derived from the quantification of the peaks, yields the value of 1:1 which is consistent to the stoichiometric ratio of the ZnO.

## 4. Conclusion

In conclusion, we have succeeded in synthesizing 2D ZnO nanopellets by using single precursor in non-hydrolytic phase via pyrolysis of organometallic compound. The current synthetic approach produced nanopellets with well-defined shapes. Furthermore, this method is simple, safe and producing nanopellets with high yield. Further development and extension of current synthetic strategy are being pursued on a variety of oxide materials with more advanced nanostructures.

## Acknowledgements

This work has been support by MOSTI under e-sciencefund (Project no.: 03-02-12-SF0019), techno-fund (Project no.: TF0106D212) and IRPA research grant (Project no.: 09-02-02-0032-SR0004/04-04). The authors also would like to gratefully acknowledge Normalawati Bt. Shamsudin, Ahmad Zaki B. Zaini and Suhaniza Bt. Razali from the Electron Microscopy Unit (UKM) for their assistance in the TEM characterization.

## References

[1] J. Wang, M.S. Gudiksen, X. Duan, Y. Cui, C.M. Lieber, Highly polarized photoluminescence and photodetection from single indium phosphide nanowires, Science 293 (2001) 1455–1457.
[2] Z. Zhong, F. Qian, D. Wang, C.M. Lieber, Synthesis of p-type gallium nitride nanowires for electronic and photonic nanodevices, Nanoletters 3 (3) (2003) 343–346.
[3] J. Hahm, C.M. Lieber, Direct ultrasensitive electrical detection of DNA and DNA sequence variations using nanowire nanosensors, Nanoletters 4 (1) (2004) 51–54.
[4] A.P. Alivisatos, Semiconductor clusters, nanocrystals, and quantum dots, Science 271 (1996) 933–937.
[5] C. Burda, X. Chen, R. Narayanan, M.A. El-Sayed, Chemistry and properties of nanocrystals of different shapes, Chem. Rev. 105 (2005) 1025–1102.
[6] N.B. Zhitenev, T.A. Fulton, A. Yacob, H.F. Hess, L.N. Pfeiffer, K.W. West, Imaging of localized electronic states in the quantum Hall regime, Nature 404 (2000) 473–476.
[7] Y.W. Suen, L.W. Engel, M.B. Santos, M. Shayegan, D.C. Tsui, Observation of a Î½ = 1/2 fractional quantum Hall state in a double-layer electron system, Phys. Rev. Lett. 68 (1992) 1379–1382.
[8] H.L. Stormer, Fractional quantum Hall effect today, Solid State Commun. 107 (1998) 617–620.
[9] H.L. Stormer, R.R. Du, W. Kang, D.C. Tsui, L.N. Peeiffer, K.W. Baldwin, K.W. West, The fractional quantum Hall effect in a new light, Semicond. Sci. Technol. 9 (1994) 1853–1858.
[10] F. Li, Y. Ding, P. Gao, X. Xin, Z.L. Wang, Single-crystal hexagonal disks and rings of ZnO: low-temperature, large-scale synthesis and growth mechanism, Angew. Chem. 116 (2004) 5350–5354.
[11] J. Park, K. An, Y. Hwang, J. Park, H. Noh, J. Kim, J. Park, N. Hwang, T. Hyeon, Ultra-large-scale syntheses of monodisperse nanocrystals, Nat. Mater. 3 (12) (2004) 891–895.
[12] Y. Sun, B. Mayers, T. Herricks, Y. Xia, Polyol synthesis of uniform silver nanowires: a plausible growth mechanism and the supporting evidence, Nanoletters 3 (2003) 955–960.
[13] M. Law, L.E. Johnson, R. Saykally, P. Yang, Nanowire dye-sensitized solar cells, Nat. Mater. 4 (6) (2005) 455–459.
[14] Z.L. Wang, Nanostructures of zinc oxide, Mater. Today 7 (6) (2004) 26–33.
[15] H. Cao, J.Y. Xu, D.Z. Zhang, S.H. Chang, S.T. Ho, E.W. Seelig, X. Liu, R.P.H. Chang, Spatial confinement of laser light in active random media, Phys. Rev. Lett. 84 (2000) 5584–5587.
[16] D.M. Bagnall, Y.F. Chen, Z. Zhu, T. Yao, S. Koyama, M.Y. Shen, T. Goto, Optically pumped lasing of ZnO at room temperature, Appl. Phys. Lett. 70 (1997) 2032–2230.
[17] P. Yu, Z.K. Tang, K.L. Wong, M. Kawasaki, A. Ohtomo, H. Koinuma, Y. Segawa, Room-temperature gain spectra and lasing in microcrystalline ZnO thin films, J. Cryst. Growth 184/185 (1998) 601–604.
[18] Y. Kayamura, Quantum-size effects of interacting electrons and holes in semiconductor microcrystals with spherical shape, Phys. Rev. B 38 (1988) 9797–9805.
[19] W. Wegscheider, L.N. Pfeiffer, M.M. Dignam, A. Pinczuk, K.W. West, S.L. McCall, R. Hull, Lasing from excitons in quantum wires, Phys. Rev. Lett. 71 (1993) 4071–4074.
[20] M.A. Garcia, J.M. Merino, E.F. Pinel, A. Quesada, J. Venta, M.L.R. Gonzalez, G.R. Castro, P. Crespo, J. Llopis, J.M. G-Calbet, A. Hernando, Magnetic properties of ZnO nanoparticles, Nanoletters 7 (2007) 1489–1494.
[21] M.H. Huang, S. Mao, H. Feick, H. Yan, Y. Wu, H. Kind, E. Weber, R. Russo, P. Yang, Room-temperature ultraviolet nanowire nanolasers, Science 292 (2001) 1879–1897.
[22] X. Wang, J. Song, J. Liu, Z.L. Wang, Direct-current nanogenerator driven by ultrasonic waves, Science 316 (2007) 102–105.
[23] P. Yang, The chemistry and physics of semiconductor nanowires, Mater. Res. Bull. 30 (2005) 85–91.
[24] L.E. Greene, M. Law, D.H. Tan, M. Montano, J. Goldberger, G. Somorjai, P. Yang, General route to vertical ZnO nanowire arrays using textured ZnO seeds, Nanoletters 5 (7) (2005) 1231–1236.
[25] G. Shen, J.H. Cho, J.K. Yoo, G.C. Yi, C.J. Lee, Synthesis and optical properties of S-doped ZnO nanostructures: nanonails and nanowires, J. Phys. Chem. B 109 (2005) 5491–5496.
[26] N. Garti, A. Aserin, I. Tiunova, M. Fanun, A DSC study of water behavior in water-in-oil microemulsions stabilized by sucrose esters and butanol, Colloid Surf. A 170 (2000) 1–18.
[27] P.S. Khiew, N.M. Huang, S. Radiman, M.S. Ahmad, Synthesis of NiS nanoparticles using a sugar–ester nonionic water-in-oil microemulsion, Mater. Lett. 58 (2004) 516–521.
[28] P.S. Khiew, S. Radiman, N.M. Huang, M.S. Ahmad, Preparation and characterization of ZnS nanoparticles synthesized from chitosan laurate micellar solution, Mater. Lett. 59 (2005) 989–993.
[29] N.M. Huang, S. Radiman, P.S. Khiew, P. Laggner, C.S. Kan, In situ templating of PbS nanorods in reverse hexagonal liquid crystal, Colloids Surf. A 247 (2004) 55–60.
[30] P.S. Khiew, S. Radiman, N.M. Huang, M.S. Ahmad, Synthesis and characterization of copper sulfide nanoparticles in hexagonal phase lyotropic liquid crystal, J. Cryst. Growth 268 (2004) 227–237.

[31] P.S. Khiew, S. Radiman, N.M. Huang, M.S. Ahmad, Studies on the growth and characterization of CdS and PbS nanoparticles using sugar–ester nonionic water-in-oil microemulsion, J. Cryst. Growth 254 (2003) 235–243.
[32] P.S. Khiew, S. Radiman, N.M. Huang, M.S. Ahmad, In situ polymerization of conducting polyaniline in bicontinuous cubic phase of lyotropic liquid crystal, Colloids Surf. A-Physicochem. Eng. Asp. 247 (2004) 35–40.
[33] N.M. Huang, C.S. Kan, P.S. Khiew, S. Radiman, Single w/o microemulsion templating of CdS nanoparticles, J. Mater. Sci. 39 (2004) 2411–2415.
[34] P.S. Khiew, N.M. Huang, S. Radiman, M.S. Ahmad, Synthesis of NiS nanoparticles using a sugar–ester nonionic water-in-oil microemulsion, Mater. Lett. 58 (2004) 762–767.
[35] S. Hirano, K. Masuya, M. Kuwabara, Multi-nucleation-based formation of oriented zinc oxide microcrystals and films in aqueous solutions, J. Phys. Chem. B 108 (2004) 4576–4578.
[36] C.L. Kuo, T.J. Kuo, M.H. Huang, Hydrothermal synthesis of ZnO microspheres and hexagonal microrods with sheetlike and platelike nanostructures, J. Phys. Chem. B 109 (43) (2005) 20115–20121.
[37] T. Yoshida, M. Tochimoto, D. Schlettwein, D. Wohrle, T. Sugiura, H. Minoura, Self-assembly of zinc oxide thin films modified with tetrasulfonated metallophthalocyanines by one-step electrodeposition, Chem. Mater. 11 (1999) 2657–2667.
[38] N. Pinna, K. Weiss, H.S. Kongehl, W. Vogel, J. Urban, M.P. Pileni, Triangular CdS nanocrystals: synthesis, characterization, and stability, Langmuir 17 (2001) 7982–7987.
[39] P. Fons, H. Tampo, A.V. Kolobov, M. Ohkubo, S. Niki, J. Tominaga, R. Carboni, F. Boscherini, S. Friedrich, Direct observation of nitrogen location in molecular beam epitaxy grown nitrogen-doped ZnO, Phys. Rev. Lett. 96 (2006) 045504–045505.
[40] W.S. Chiu, S. Radiman, M.H. Abdullah, P.S. Khiew, N.M. Huang, R. Abd-Shukor, One pot synthesis of monodisperse $Fe_3O_4$ nanocrystals by pyrolysis reaction of organometallic compound, Mater. Chem. Phys. 106 (2007) 231–235.
[41] X. Peng, Mechanisms for the shape-control and shape-evolution of colloidal semiconductor nanocrystals, Adv. Mater. 15 (5) (2003) 459–463.
[42] W.W. Yu, Y.A. Wang, X. Peng, Formation and stability of size-, shape-, and structure-controlled CdTe nanocrystals: ligand effects on monomers and nanocrystals, Chem. Mater. 15 (2003) 4300–4308.
[43] W.W. Yu, X. Peng, Formation of high-quality CdS and other II–VI semiconductor nanocrystals in noncoordinating solvents: tunable reactivity of monomers, Angew. Chem. Int. Ed. 41 (13) (2002) 2368–2371.
[44] Z.L. Wang, X.Y. Kong, J.M. Zuo, Induced growth of asymmetric nanocantilever arrays on polar surfaces, Phys. Rev. Lett. 91 (18) (2003) 185502–185505.
[45] W.S. Chiu, S. Radiman, R. Abd-Shukor, M.H. Abdullah, P.S. Khiew, Tunable coercivity of $CoFe_2O_4$ nanoparticles via thermal annealing treatment, J. Alloy Comp. 459 (2008) 291–297.
[46] J.O. Bovin, R.L. Wallember, D. Smith, Imaging of atomic clouds outside the surfaces of gold crystals by electron microscopy, Nature 317 (1985) 47–49.
[47] S. Iijima, H. Ichihashi, Structural instability of ultrafine particles of metals, Phys. Rev. Lett. 56 (1986) 616–619.
[48] H. Zhu, R.S. Averback, Sintering processes of two nanoparticles: a study by molecular dynamics simulations, Philos. Magn. Lett. 73 (1996) 27–33.
[49] B.J. Wiley, S.H. Im, Z.Y. Li, J. McLellan, A. Siekkinen, Y. Xia, Maneuvering the surface plasmon resonance of silver nanostructures through shape-controlled synthesis, J. Phys. Chem. B 110 (2006) 15666–15675.
[50] K.L. Kelly, E. Corondo, L.L. Zhao, G.C. Sxhatz, The optical properties of metal nanoparticles: the influence of size, shape, and dielectric environment, J. Phys. Chem. B 107 (2003) 668–677.
[51] Y. Leng, Y. Zhang, T. Liu, M. Suzuki, X. Li, Synthesis of single crystalline triangular and hexagonal Ni nanosheets with enhanced magnetic properties, Nanotechnology 17 (6) (2006) 1797–1800.
[52] A.C.S. Samia, K. Hyzer, J.A. Schlueter, C. Qin, J.S. Jiang, X.D. Bader, X. Lee, Ligand effect on the growth and the digestion of Co nanocrystals, J. Am. Chem. Soc. 127 (2005) 4126–4127.
[53] X.Y. Kong, Z.L. Wang, Spontaneous polarization-induced nanohelixes, nanosprings and nanorings of piezoelectric nanobelts, Nanoletters 3 (12) (2003) 1625–1631.
[54] Joint Committee for Powder Diffraction Society (JCPDS), Powder Diffraction Database, pattern: 36-1451.
[55] C.Y. Yeh, Z.W. Lu, S. Froyen, A. Zunger, Zinc-blende? wurtzite polytypism in semiconductors, Phys. Rev. B 46 (1992) 10086–10097.
[56] C.Y. Yeh, S.H. Wei, A. Zunger, Relationships between the band gaps of the zinc-blende and wurtzite modifications of semiconductors, Phys. Rev. B 50 (1994) 2715–2718.
[57] J. Serrano, A.H. Romero, F.J. Manjón, R. Lauck, M. Cardona, A. Rubio, Pressure dependence of the lattice dynamics of ZnO: an ab initio approach, Phys. Rev. B 69 (2004) 094306–094319.
[58] J.F. Shackelford, Introduction to Material Science for Engineers, 6th ed., Pearson-Prentice Hall, USA, 2004, p. 106.
[59] E.V. Shevchenko, D.V. Talapin, H. Schnablegger, A. Kornowski, O. Festin, P. Svedlindh, M. Haase, H. Weller, Study of nucleation and growth in the organometallic synthesis of magnetic alloy nanocrystals: the role of nucleation rate in size control of $CoPt_3$ nanocrystals, J. Am. Chem. Soc. 125 (2003) 9090–9101.
[60] Q. Li, V. Kumar, Y. Li, H. Zhang, T.J. Marks, R.P.H. Chang, Fabrication of ZnO nanorods and nanotubes in aqueous solutions, Chem. Mater. 17 (2005) 1001–1006.
[61] L. Xu, Y. Guo, Q. Liao, J. Zhang, D. Xu, Morphological control of ZnO nanostructures by electrodeposition, J. Phys. Chem. B 109 (28) (2005) 13519–13522.
[62] Y. Jun, J. Lee, J. Choi, J. Cheon, Symmetry-controlled colloidal nanocrystals: nonhydrolytic chemical synthesis and shape determining parameters, J. Phys. Chem. B 109 (2005) 14795–14806.